Supporting Information

Montabana and Agard 10.1073/pnas.1318339111

SI Materials and Methods

Cloning, Protein Expression, and Purification. The TubZ gene from plasmid pBtoxis of *Bacillus thuringiensis serovar israelensis* was a kind gift of J. Pogliano (University of California at San Diego, San Diego, CA). The gene was provided cloned into pET28a, and contained the mutation L2V. This mutation was removed by site-directed mutagenesis to generate the C-terminally his-tagged construct used in our studies (WT-TubZ-pET28a). Site-directed mutagenesis on this construct was used to generate the hydrolysis-deficient mutant D269A (D269A-TubZ-pET28a). To generate the N-terminally tagged construct, TubZ was subcloned into pET151/D-TOPO (Invitrogen) (WT-TubZ-pET151). This provided a tobacco etch virus (TEV) protease cleavage site, which leaves the residues GIDPFT before the start methionine on the protein after cleavage. Untagged TubZ was then cloned from this construct using inverse PCR to remove all residues before the start methionine of TubZ. The K224A/K227A/K230A mutation and truncations 1-442, 1-460, 1-470 were then made using inverse PCR on the tagless construct (3K-TubZ, TubZ-1-442, TubZ-1-460, TubZ-1-470). All proteins were expressed in either BL21(DE3)star or BL21(RIL) cells, grown at 30 °C to OD600 ~0.5, the induced with 1 mM isopropyl-β-D-thiogalactopyranoside at 16 °C overnight. Cells were then pelleted and stored at −80 °C until purification.

WT-TubZ-pET28a was purified by lysing a 1-L cell pellet in lysis buffer (100 mM Tris-Cl pH 8.5, 300 mM NaCl), then centrifuged at 35,000 × *g* for 45 min, and the supernatant was then mixed with NiNTA resin, for 1 h at 4 °C. Protein was then eluted (100 mM Tris·Cl pH 8.5, 300 mM imidazole, 100 mM NaCl), and loaded onto an HiTrap Q HP column (100 mM Tris·Cl pH 8.5, 50–1,000 mM NaCl gradient) followed by size-exclusion chromatography (S200 16/60, 100 mM Tris·Cl, 150 mM NaCl, 1 mM EDTA, 1 mM NaN_3). All protein was dialyzed into HMK100 buffer (50 mM Hepes pH 7.7, 100 mM KAc, 5 mM $MgAc_2$) before biochemistry or electron microscopy.

D269A-TubZ-pET28a was purified by lysing a 2-L cell pellet, resuspended in lysis buffer [50 mM Hepes pH 7.7, 20 mM KAc, cOmplete EDTA-free protease inhibitor mixture (Roche Applied Science), 1 mM DTT], then centrifuged at 35,000 × *g* for 45 min. The supernatant was then mixed with NiNTA resin, for 1 h at 4 °C. Protein was then eluted (50 mM Hepes pH 7.7, 20 mM KAc, 300 mM imidazole), and then run on a size-exclusion column (50 mM Hepes pH 7.7, 20 mM KAc).

WT-TubZ-pET151 was purified by lysing a 1-L cell pellet, resuspended in lysis buffer [50 mM Hepes pH 7.7, 300 mM KAc, 5 mM $MgAc_2$, 10% (vol/vol) glycerol, 10 mM thioglycerol], then centrifuged at 35,000 × *g* for 40 min. The supernatant was then mixed with NiNTA resin, for 1 h at 4 °C. Protein was then eluted [50 mM Hepes pH 7.7, 300 mM KAc, 5 mM $MgAc_2$, 10% (vol/vol) glycerol, 10 mM thioglycerol, 300 mM imidazole], and cleaved overnight at room temperature with TEV protease. Protein was then then run on a size exclusion column [50 mM Hepes pH 7.7, 300 mM KAc, 5 mM $MgAc_2$, 10% (vol/vol) glycerol, 10 mM thioglycerol].

Untagged TubZ was purified by was purified by lysing a 1-L cell pellet, resuspended in lysis buffer (50 mM Hepes pH 7.7, 100 mM KCl, 5 mM $MgCl_2$, 1 mM DTT), then centrifuged at ~94,000 × *g* for 1 h. Two ammonium sulfate cuts were performed, at 25% and 40% saturation. The 40% saturation pellet was resuspended and run over a PD-10 desalting column (GE Healthcare) (50 mM Hepes pH 7.7, 100 mM KCl, 10 mM $MgCl_2$, 1 mM DTT). The desalted fraction was then spun at 126,000 × *g* for 15 min to remove aggregates. The supernatant was then mixed with 10 mM GTP and then spun again for 15 min. The pellet was then resuspended and dialyzed overnight in 1 L depolymerization buffer (50 mM Hepes pH 7.7, 20 mM KAc, 5 mM EDTA). Protein was then run on a size-exclusion column in same buffer. Collected fractions were then dialyzed against 2 L HMK100 buffer (50 mM Hepes pH 7.7, 100 mM KAc, 5 mM $MgAc_2$) overnight, and then for 4 h in 2 L fresh buffer.

TubZ-1-470 was purified in a manner to similar to wild-type untagged TubZ, but because of its lower ability to polymerize, the polymerization step was inefficient. Both supernatant and pellet of the polymerization were dialyzed overnight, and then run on a size-exclusion column followed by a HiTrap Q HP column (50 mM Hepes pH 7.7, 5 mM EDTA. 20–1000 mM KAc gradient). Collected Fractions were dialyzed as above.

The 3K-TubZ, TubZ-1-442, and TubZ-1-460 proteins were purified in a similar manner to wild-type untagged TubZ. The first ammonium sulfate cut was performed at 20% saturation for 3K-TubZ, but 25% saturation for all others. After the second cut, the pellet was resuspended and either desalted (3K-TubZ), or dialyzed overnight (TubZ-1-442, TubZ-1-460). The resuspension was then run on a HiTrap Q HP column (50–1,000 mM KCl or KAc gradient), followed by size exclusion. TubZ-1-442 and TubZ-1-460 were dialyzed as above to remove EDTA from their buffers.

TubZ-Bt Polymerization and Sedimentation Assays. Ninety-degree light-scattering experiments were measured using stopped-flow system designed in-house. An excitation wavelength of 530 nm was used. Polymerization was initiated by mixing 2× TubZ protein with 2× nucleotide, or buffer. The final concentration was 3 μM TubZ, 0.5 mM nucleotide. All proteins, with the exception of D269A-TubZ-pET28a, were dialyzed overnight into HMK100 buffer before polymerization. Because of its tendency to aggregate in polymerization buffer, reagents were added to D269A-TubZ-pET28a before polymerization to match HMK100 buffer.

For sedimentation assays, 6 μM WT-TubZ-pET28a, WT-TubZ-pET151, or untagged WT-TubZ was assembled with 1 mM GTP or GTPγS in HMK100 buffer for 10 min at room temperature in a 100-μL volume. The reactions were then centrifuged in a Beckman TLA100 rotor at ~117,000 × *g* for 30 min. Pellets were resuspended in loading buffer, and both pellet and supernatant were analyzed on 4–12% SDS/PAGE with SimplyBlue Safe Stain (Invitrogen).

Electron Microscopy. Initial morphology analysis was done using negative-stain EM. About 5-μL of sample protein (2–8 μM) was preincubated at room temperature with nucleotide and applied to a glow-discharged carbon-coated grid. The exception to this is samples that were incubated on the grid to stabilize two-stranded filaments. In this case, about 4.5 μL of sample protein was applied to the grid, and 0.5 μL GTP was added, and allowed to incubate for 10–30 s before washing and staining. Samples were negatively stained with 0.75% uranyl formate, and imaged on Tecnai T12 Spirit (FEI) operating at 120 kV.

Cryo-electron microscopy (cryo-EM) samples were prepared on glow-discharged C-flat (Protochips) holey carbon grids that were plunge-frozen in liquid ethane using a Vitrobot (FEI). For the four-stranded reconstruction, wild-type untagged TubZ ~8–12 μM was incubated in the presence of saturating GTP (1 mM) for 4–6 min at room temperature before sample application and plunge-freezing. For the two-stranded reconstruction, WT-TubZ-pET151 ~8–10 μM was preheated at 37 °C, and polymerization

was initiated with saturating GTPγS (1 mM) and incubated for 30 s at room temperature before sample application and plunge-freezing. Cryo-EM data were obtained on a Tecnai F20 operating at 200 kV with an 8k × 8k TemCam-F816 camera (TVIPS) with a pixel size of 0.94 Å per pixel for the four-stranded reconstruction, and 1.203 Å per pixel for the two-stranded reconstruction.

Data Processing and Helical Reconstruction for Four-Stranded Reconstruction. In total, 414 images were collected. The defocus and astigmatism parameters of the images were determined using CTFFIND3 (1), and each micrograph was CTF-multiplied using SPIDER (2); additionally, micrographs were separately corrected using a Weiner filter with in-house software. Particles were boxed out in ∼481 Å segments, overlapping by ∼395 Å. Particles were recentered with respect to the helix axis by integer pixel shifts after several initial rounds of reconstruction. Iterative helical real space refinement was performed via the method outlined in Egelman (3), although modified to use the gold-standard method (4). An initial reconstruction was done using standard Iterative Helical Real Space Refinement methodology using a low-pass filtered cylinder as an initial model. Particle alignment was done with particles boxed from CTF-multiplied images, and back-projections were performed using fully CTF-corrected particles. Particles that were obviously misaligned based on angle, shifts, or polarity were determined at each round, and not used for the back-projection. Of 38,186 particles, 27,415 were used in the final reconstruction. After each round of reconstruction, the volume was both low-pass and high-pass filtered and then used as the reference model for the next round. After several initial rounds were done at 4× bin, particles were recentered with respect to the helix axis by integer pixel shifts and masked with a cosine-edge mask. Several more rounds of reconstruction were done, and then 2× bin particles were used. The mask and particle size was decreased twice, and then final rounds of refinement of the structure were performed on unbinned particles, only allowing a search of 5° around previously determined alignment parameters. The final box size was ∼241 Å. After this reconstruction was substantially refined, it was low-pass filtered to 50 Å. This low-pass filtered reconstruction was then used as an initial model for alignment of two independent subsets, which were consequently aligned and back-projected. A full model using both subsets of data were back-projected using the independently determined alignment parameters of the subsets to determine the helical parameters, and then these helical parameters were applied to the back projections of the two subsets to determine resolution. The full model, which had been helically symmetrized before being low-pass filtered to the determined resolution, as well as high-pass filtered, was used as the reference model for the next round for both subsets, to retain appropriate orientation of the filaments from round to round. The helical symmetry was allowed to refine throughout this process.

Molecular Dynamics Flexible Fitting. A chimeric PDB of two PDBs was first created using PyMol (5) of residues 76–118 and 383–414 of PDB ID code 2XKA chain F and residues of 1–75, 119–382, and GDP of PDB ID code 2XKB chain C to have residues 1–414 present in a starting model. This PDB was then fit into the four-stranded reconstruction, which had been low-pass filtered to 6.9 Å and high-pass filtered to 30 Å, as well b-factor scaling of ∼−309 Å. This rigid body fit was doing using "Fit into Map" in Chimera (6). Additional subunits were then created using known helical symmetry to make a full model containing 16 subunits. This full PDB was then prepared for molecular dynamics flexible fitting (MDFF) (7) using visual molecular dynamics (8). MDFF was run with the GDP molecule restrained for 300 ps with a scaling factor ξ of 1 followed by 2,000 minimization at 300 K. An additional 9,000-step energy minimization was then done at a scaling factor ξ of 10. CHARMM force-field parameters were used throughout. To make a finalized version of the molecular model, one subunit was from the MDFF simulation was chosen based both on correlation with the EM map in Chimera (6) and also by visual inspection. Chimera was used to change residue V2 to L, as this residue mutated in the crystal structure but not in the protein used for EM, and we wished to reflect this in our model. This model was redocked into the EM map and helical symmetry parameters were used to create additional subunits.

Data Processing and Helical Reconstruction for Two-Stranded Reconstruction. In total, 348 images were collected, and CTF determination and correction and reconstruction were performed essentially as above. The particles were boxed out in ∼582 Å segments, overlapping by ∼532 Å. The final box size was ∼241 Å. Of 17,828 particles, 11,896 were used in the final reconstruction. Most particles that were discarded were because of an inability to align with the correct polarity.

1. Mindell JA, Grigorieff N (2003) Accurate determination of local defocus and specimen tilt in electron microscopy. *J Struct Biol* 142(3):334–347.
2. Frank J (1996) *Three-Dimensional Electron Microscopy of Macromolecules* (Academic Press, San Diego).
3. Egelman EH (2007) The iterative helical real space reconstruction method: Surmounting the problems posed by real polymers. *J Struct Biol* 157(1):83–94.
4. Scheres SH, Chen S (2012) Prevention of overfitting in cryo-EM structure determination. *Nat Methods* 9(9):853–854.
5. The PyMOL Molecular Graphics System, Version 1.7rc1 (Schrödinger, LLC).
6. Pettersen EF, et al. (2004) UCSF Chimera—A visualization system for exploratory research and analysis. *J Comput Chem* 25(13):1605–1612.
7. Trabuco LG, Villa E, Mitra K, Frank J, Schulten K (2008) Flexible fitting of atomic structures into electron microscopy maps using molecular dynamics. *Structure* 16(5): 673–683.
8. Humphrey W, Dalke A, Schulten K (1996) VMD: Visual molecular dynamics. *J Mol Graph* 14(1):33–38, 27–28.

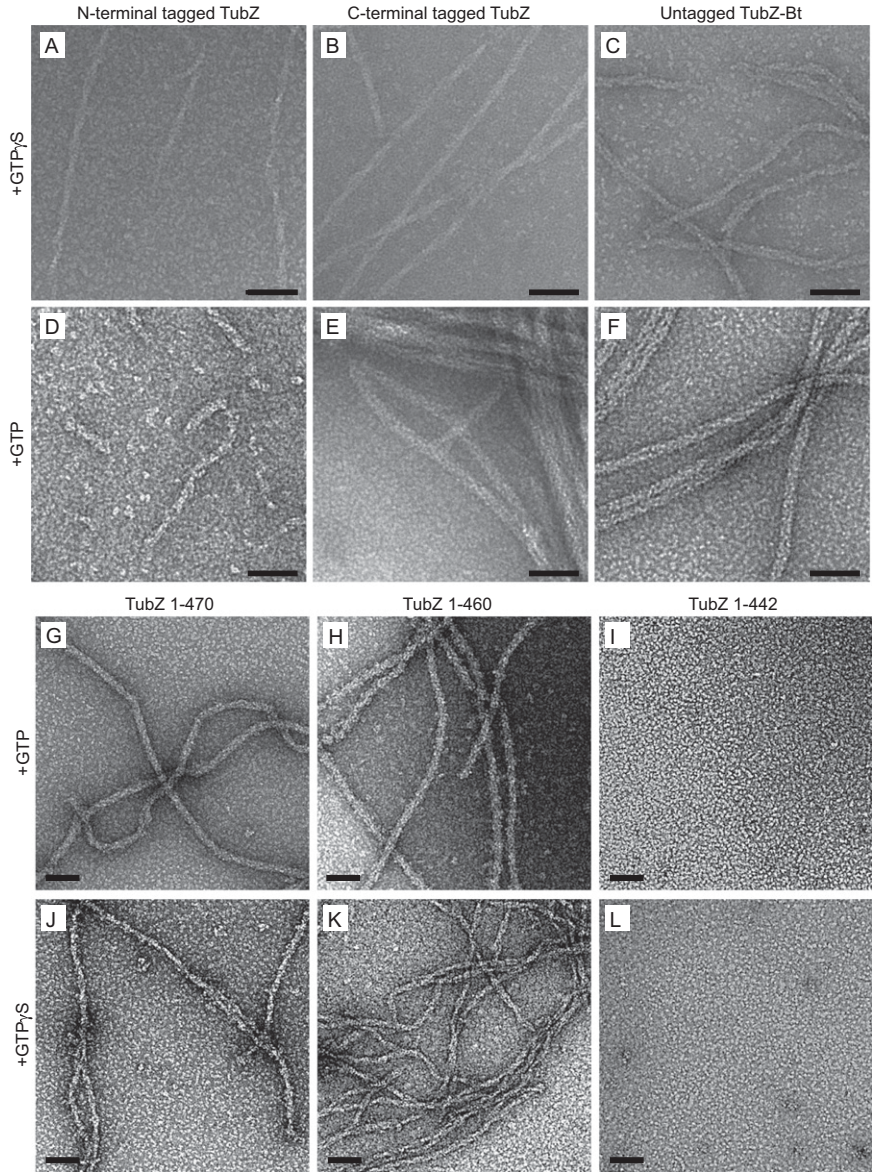

Fig. S1. Morphology of tagged, untagged, and truncated TubZ-Bt filaments. Electron micrographs of negatively stained EM, of N-terminally tagged TubZ in the presence of GTPγS (*A*) or GTP (*D*), C-terminally tagged TubZ in the presence of GTPγS (*B*) or GTP (*E*), or untagged TubZ in the presence of GTPγS (*C*) or GTP (*F*). Electron micrographs of negative-stain EM of TubZ 1-470 in the presence of GTP (*G*) or GTPγS (*J*), TubZ 1-460 in the presence of GTP (*H*) or GTPγS (*K*), or TubZ 1-442 in the presence of GTP (*I*) or GTPγS (*L*). (Scale bars, 500 Å.)

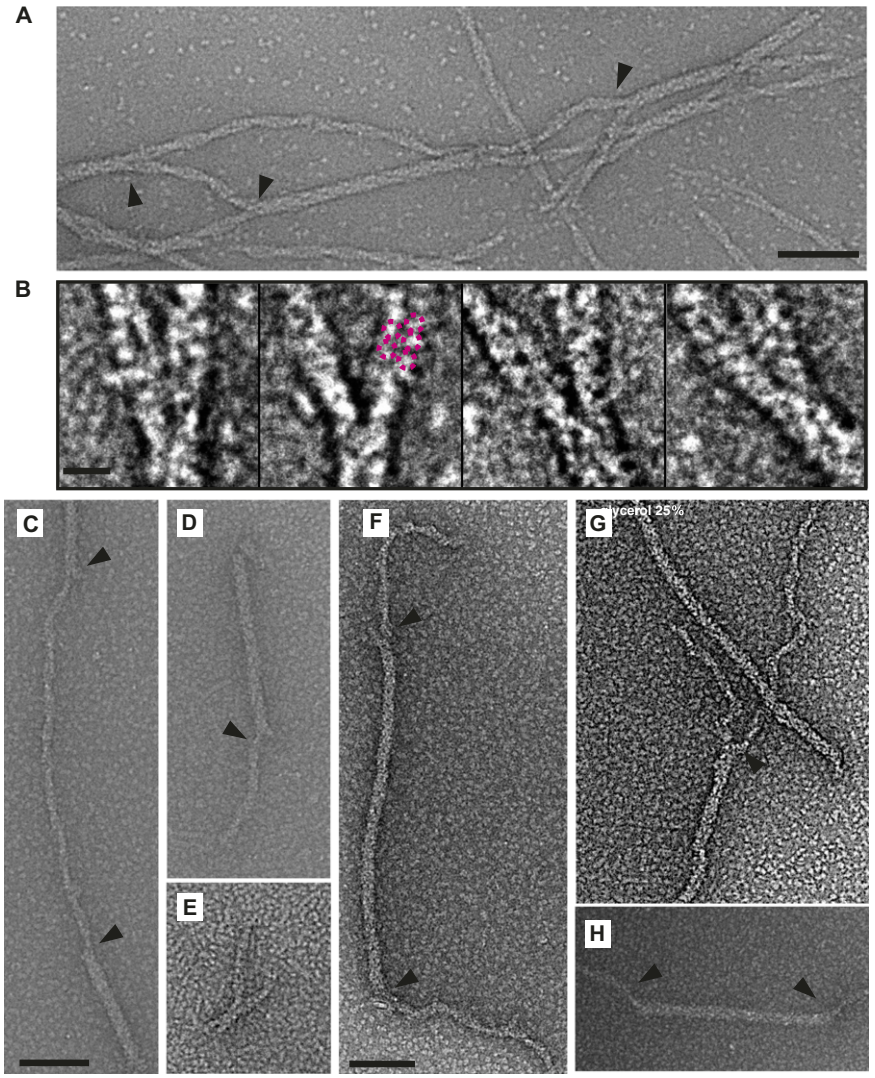

Fig. S2. Examples of the ability of TubZ to convert between filament morphologies. (*A*) Electron micrograph of negative-stain EM of untagged TubZ assembled in the presence of GTPγS. (Scale bar, 500 Å.) (*B*) Boxed particles of the same condition displaying examples of forked transitions from four- to two-strands. Pink circles highlight visible puncta that indicate that the two-stranded filaments emerging from forks have the same morphology as free two-stranded filaments. (Scale bar, 100 Å.) (*C–E*) Electron micrographs of negative-stain EM of untagged TubZ assembled in the presence of GTP, grown on the grid for either 10 s (*C*), 20 s (*D*), or 30 s (*E*). (Scale bar, 500 Å.) (*F–H*) Electron micrographs of negative-stain EM of untagged TubZ assembled in the presence of GTP, grown in the presence of 25% glycerol. (Scale bar, 500 Å.) Black arrows indicate transition points.

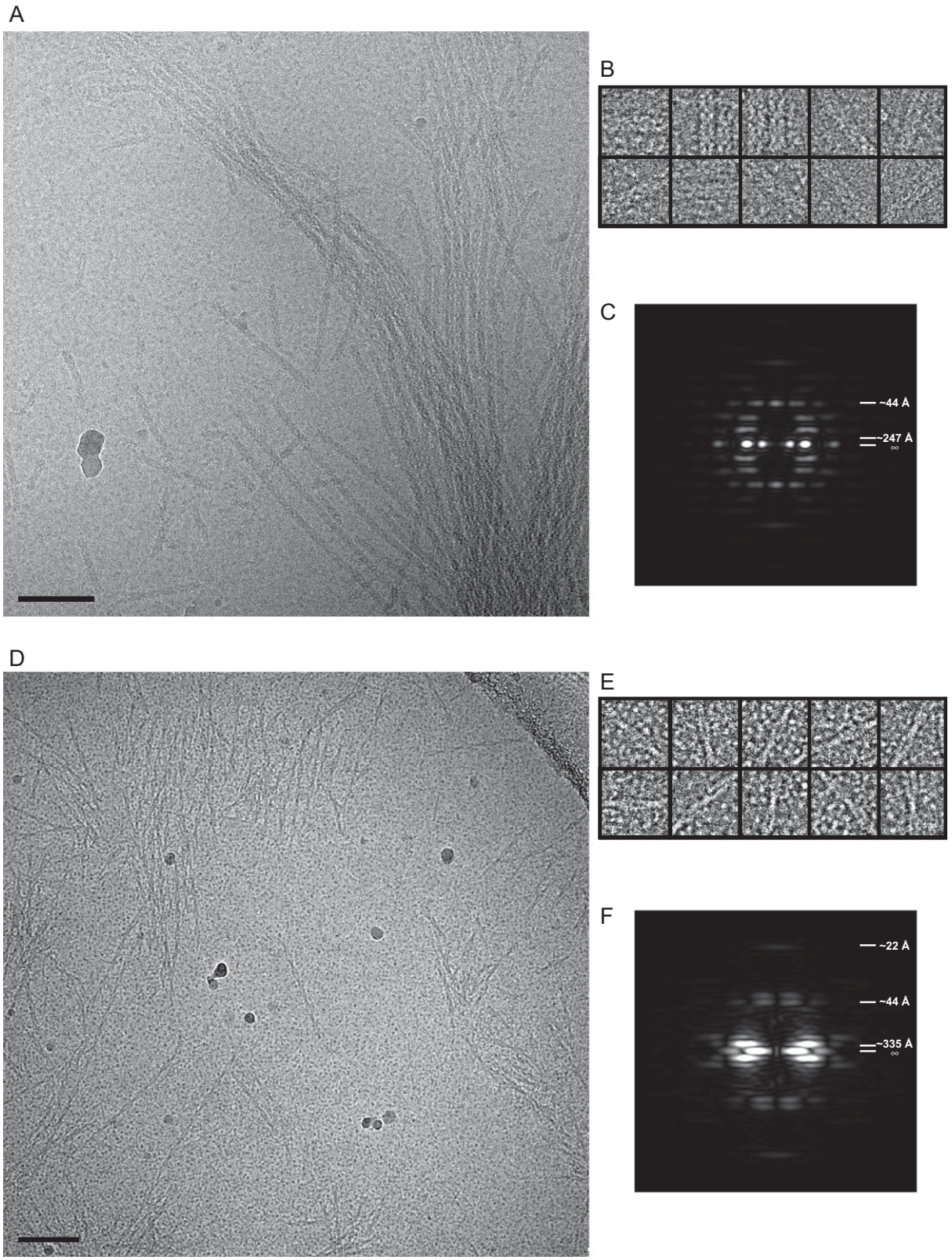

Fig. S3. Data from cryo-EM of four-stranded and two-stranded TubZ-Bt filaments. Electron micrographs of cryo-EM of (*A*) untagged TubZ-Bt in the presence of GTP, 8× binned, 1.9 μm underfocus or (*D*) N-terminally tagged TubZ-Bt in the presence of GTPγS, 8× binned, 3.4 μm underfocus. (Scale bars, 100 nm.) Gallery of select particles at 4× bin of (*B*) untagged TubZ-Bt:GTP and (*E*) N-terminally tagged TubZ-Bt:GTPγS. (Box sizes in *B* and *E* are ∼120 Å and ∼140 Å, respectively.) Power spectra of (*C*) untagged TubZ-Bt:GTP particle set or (*F*) N-terminally tagged TubZ-Bt:GTPγS particle set from respective 2D averages of particles.

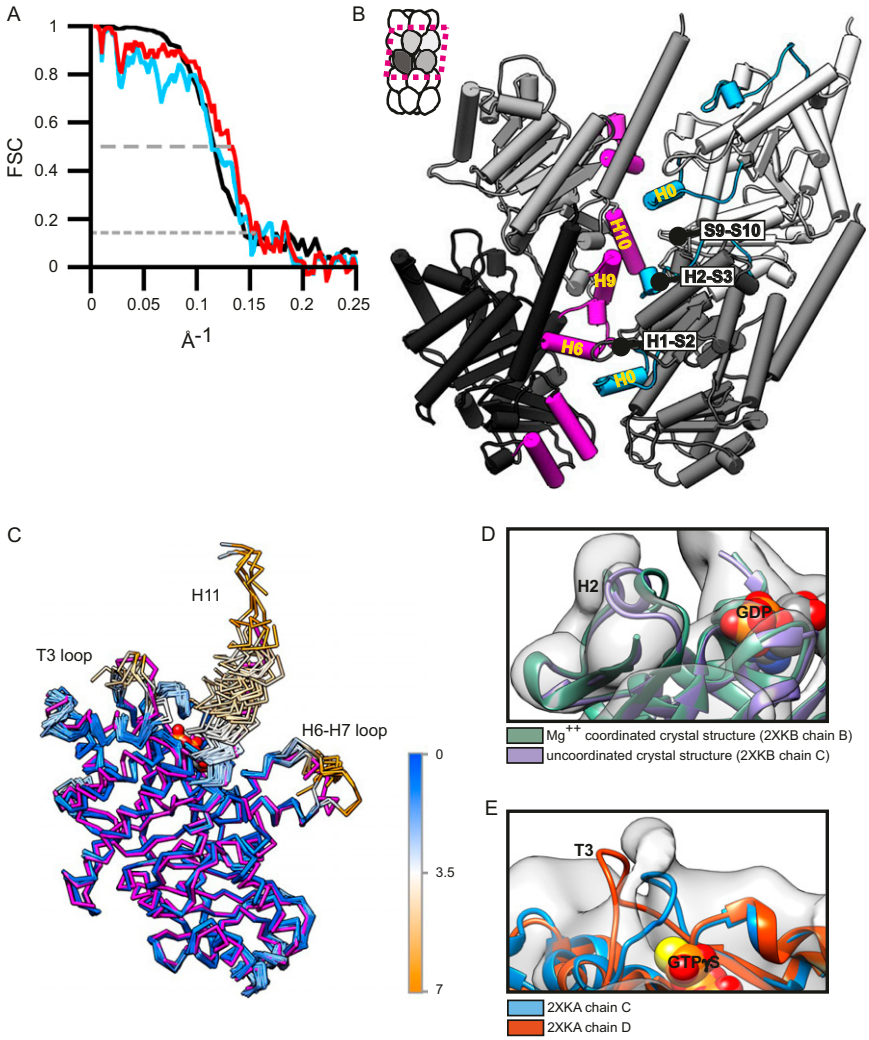

Fig. S4. Analysis of the four-stranded filament reconstruction. (*A*) Fourier shell correlation (FSC) curve plotting resolution of the four-stranded filament (black), resolution of the experimental map versus the MDFF pseudoatomic model (red), and resolution of the experimental map versus the starting pseudoatomic model (blue). Resolution is 8.6 Å at 0.5 cut-off and 6.9 Å at 0.143 cut-off for the experimental map, 7.6 Å at 0.5 cut-off for the pseudoatomic MDFF model, and 8.77 Å at 0.5 cut-off for the starting pseudoatomic model. (*B*) Highlight of potential interaction interfaces revealed by the pseudoatomic model, using the MDFF model. (*C*) MDFF model (magenta) overlaid with all published chains of TubZ (PBD ID codes 3M89, 3M8K, 2XKA[A:F], and 2XKB[A:L]). All structures are aligned with chain A of PDB ID code 2XKA using residues 1–80 and 102–383. Crystal structures are colored by RMSD from chain A. (*D*) Close-up of GTP binding pocket. Fitting of a structure (2XKB:B) in which H2 is coordinated with Mg^{2+} (green) in an "in" position, and of a structure (2XKB:C) in which H2 is uncoordinated with Mg^{2+} (purple), in an "out" position, demonstrating that density corresponds with an uncoordinated "out" H2. (*E*) Close up of T3 loop. Fitting of the two T3 loop conformations seen in crystal structures 2XKA:C (blue) and 2XKA:D (orange).

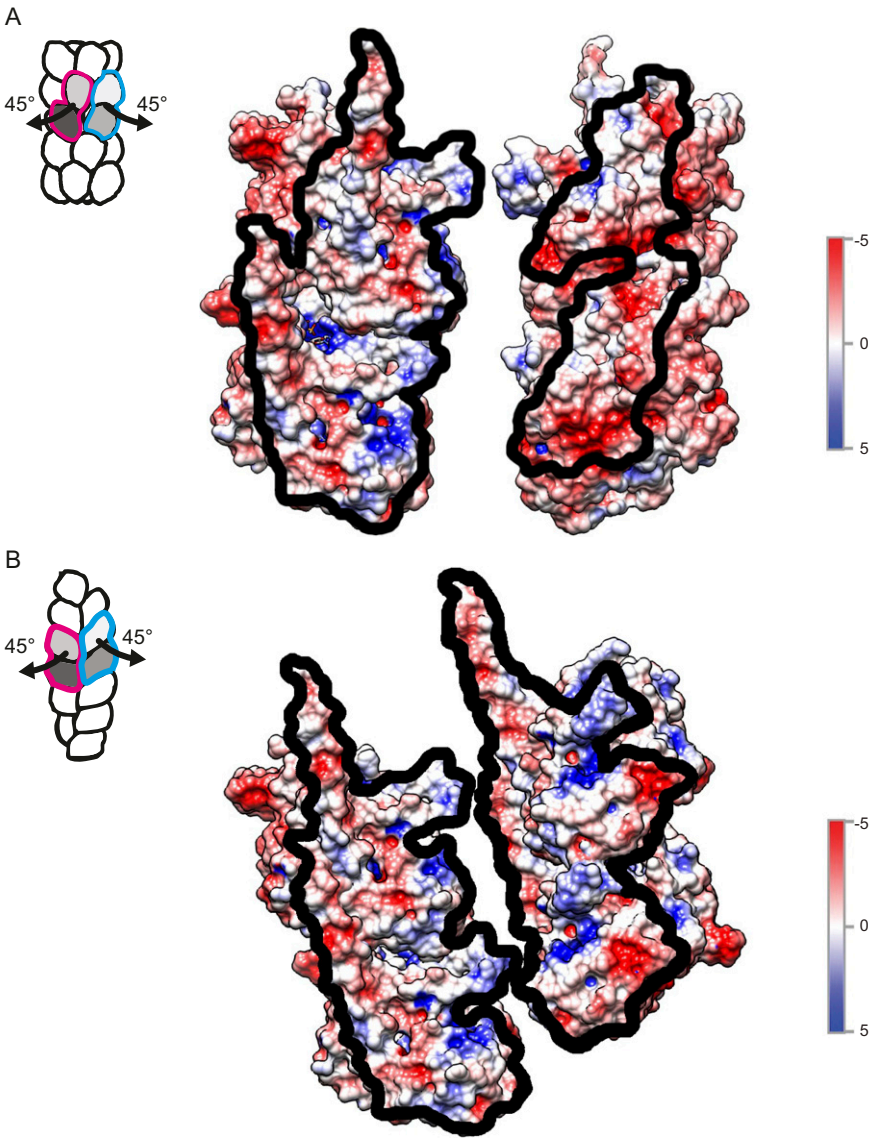

Fig. S5. Comparison of the interactions of the two- and four-stranded interfaces. (*A* and *B*) Four-stranded and two-stranded electrostatic interfaces, respectively, broken apart with each strand rotated outward 45°. Structure used for representation in both is MDFF model from the four-stranded reconstruction.

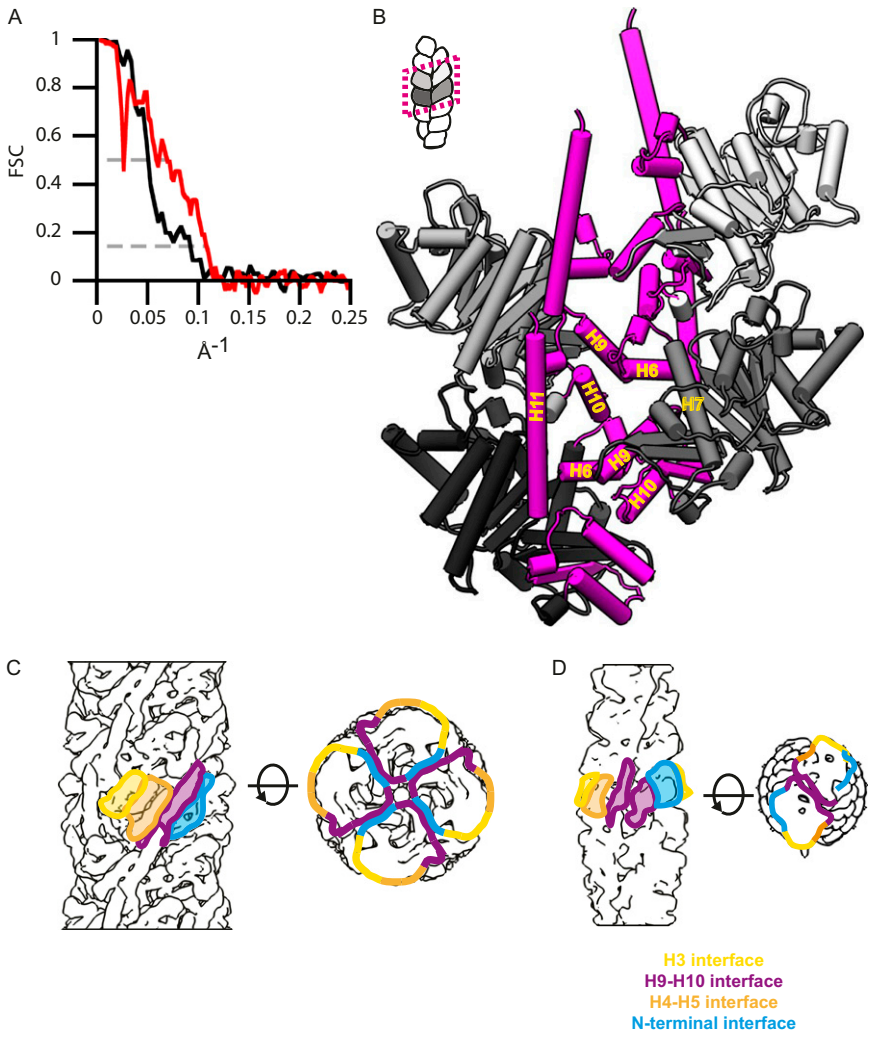

Fig. S6. Analysis of the two-stranded filament reconstruction. (*A*) FSC curve plotting resolution of the two-stranded filament (black) and resolution of the experimental map versus the pseudoatomic model (red). Resolution is 19.7 Å at 0.5 cut-off and 10.8 Å at 0.143 cut-off for the experimental map, and 14.4 Å at 0.5 cut-off for the pseudoatomic model using PDB ID code 2XKA chain F. (*B*) Highlight of potential interaction interfaces revealed by the pseudoatomic model. (*C* and *D*) Cartoon diagrams of different interfaces observed in the four- and two-stranded reconstructions respectively: residues 0–80 and 236–257 are colored in blue, 81–129 in gold, 130–212 in orange, and 213–235 and 258–414 in magenta.

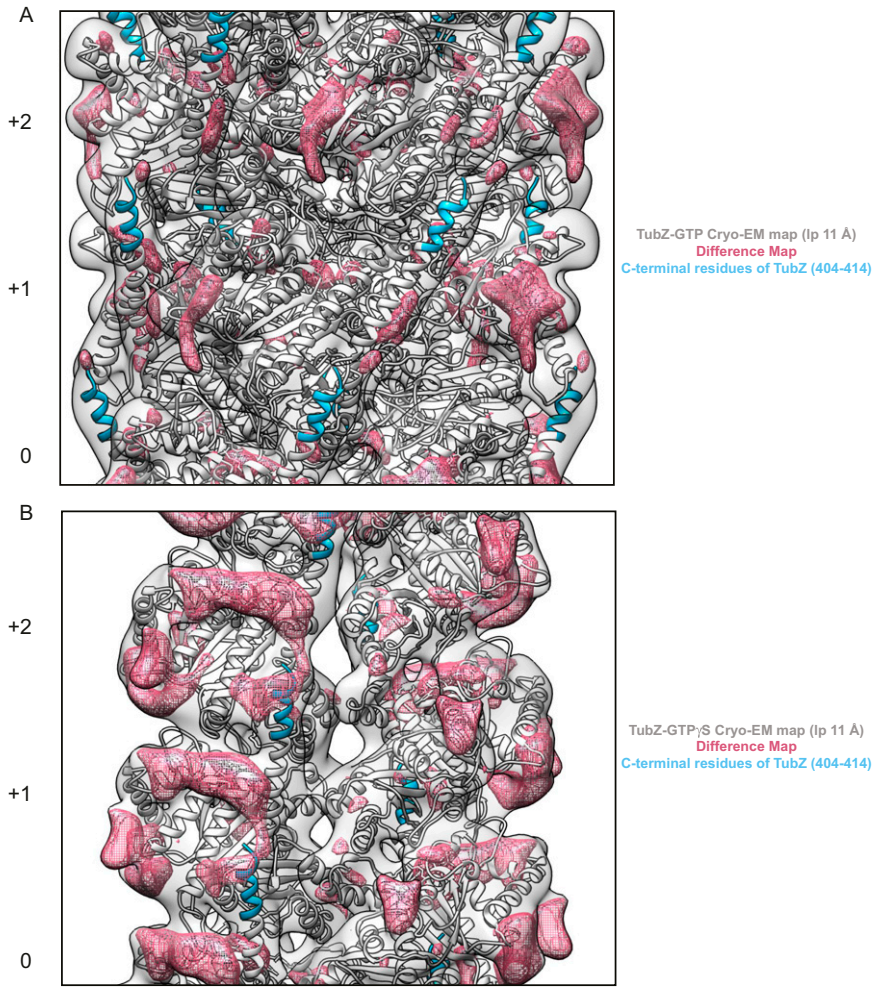

Fig. S7. Difference maps of four- and two-stranded filament reconstructions highlighting location of C-terminal tail density. (*A*) Difference map between four-stranded reconstruction and pseudoatomic map, both filtered at 11 Å. Density differences indicated in pink, and end of C-terminal tail (residues 404–414) indicated in blue. (*B*) Difference map between two-stranded reconstruction and pseudoatomic map, both filtered at 11 Å. Density differences indicated in pink, and end of C-terminal tail (residues 404–414) indicated in blue. Psuedo-atomic models were made using the MDFF model from the four-stranded reconstruction.

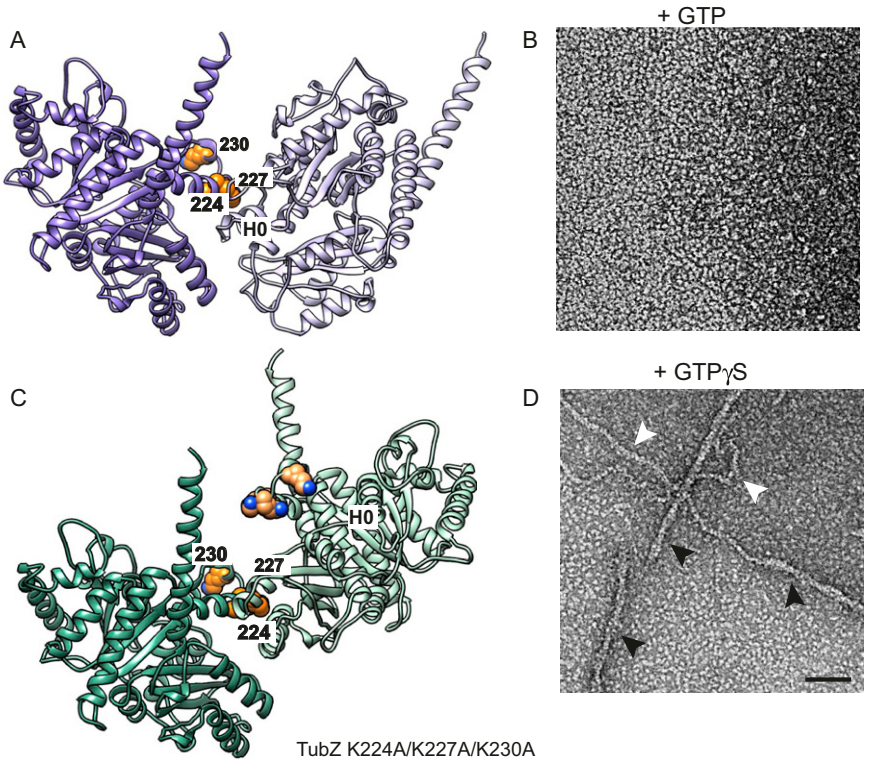

Fig. S8. Mutants to lateral four-stranded interface mainly affect four-stranded filament formation. (*A*) Location of K224, K227, and K230 in the four-stranded interface, highlighted in orange spheres. (*B*) Electron micrograph of negative-stain EM of K224AK227AK230A TubZ triple mutant in the presence of GTP, showing no assembly of TubZ filaments. (*C*) Location of K224, K227, and K230 in the two-stranded interface, highlighted in orange spheres. Structure used for representation in *A* and *C* is the MDFF model from the four-stranded reconstruction. (*D*) Electron micrograph of negative-stain EM of K224AK227AK230A TubZ triple mutant in the presence of GTPγS, showing assembly of two-stranded TubZ filaments (black arrows), and some single protofilaments (white arrows). (Scale bars in *B* and *D*, 50 nm.)

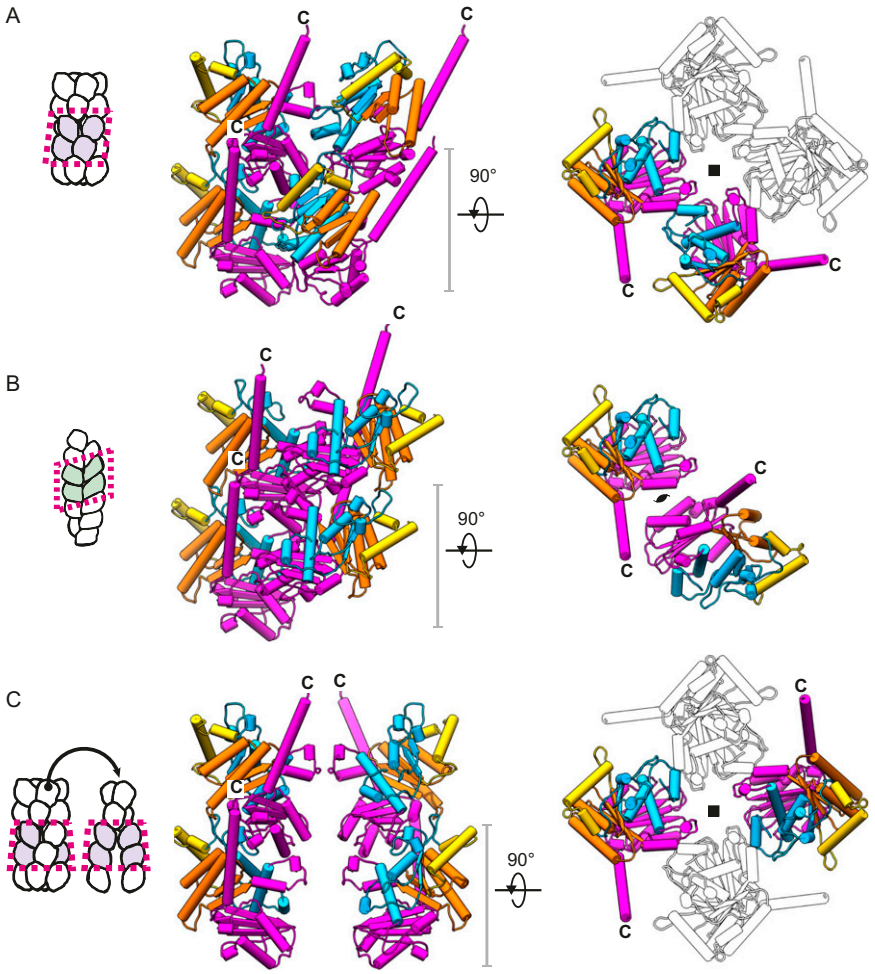

Fig. S9. Comparison of the lateral interactions of the two- and four-stranded protofilaments. (*A*) Interaction of adjacent protofilaments in the four-stranded structure. (*B*) Interaction of two-stranded filament. (*C*) Interaction of opposite protofilaments of the four-stranded structure. Structure used for representation for all is the MDFF model from the four-stranded reconstruction. Residues 0–80 and 236–257 are colored in blue, 81–129 in gold, 130–212 in orange, and 213–235 and 258–414 in magenta.

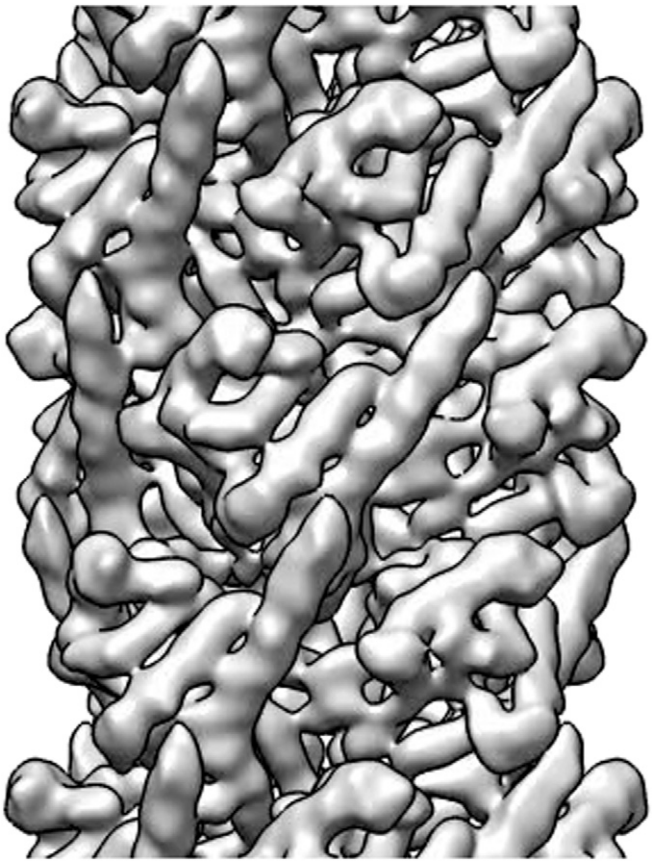

Movie S1. Movie of cryo-EM TubZ-GTP filament reconstruction. Filament has been low-pass filtered to 7 Å, a B-factor of ∼−309 applied, and high-pass filtered to 30 Å. A pseudoatomic model is fit, using a structure determined using MDFF. Residues 0–80 and 236–257 are colored in blue, 81–129 in gold, 130–212 in orange, and 213–235 and 258–414 in magenta. Unconnected density has been hidden for improved visualization. Zoom-in density has been cropped for visualization of an individual monomer using University of California, San Francisco (UCSF) Chimera.

Movie S1

Movie S2. Movie of cryo-EM TubZ-GTPγS filament reconstruction. Filament has been low-passed filtered to 11 Å, a B-factor of ∼−452 applied, and high-pass filtered to 35 Å. A pseudoatomic model is fit using PDB ID code 2XKA chain F. Residues 0–80 and 236–257 are colored in blue, 81–129 in gold, 130–212 in orange, and 213–235 and 258–414 in magenta. Unconnected density has been hidden for improved visualization. Zoom-in density has been cropped for visualization of an individual monomer using UCSF Chimera.

Movie S2